RESULTS OF THE CERN NA3 EXPERIMENT ON MUON PAIR PRODUCTION IN HADRON COLLISIONS

CEN Saclay[1]-CERN[2]- Collège de France[3]- E.P. Palaiseau[4]- LAL Orsay[5] Collaboration

J. Badier[4], J. Boucrot[5], G. Burgun[1], O. Callot[5], P. Charpentier[1], M. Crozon[3], D. Decamp[2], P. Delpierre[3], A. Diop[3], R. Dubé[5], B. Gandois[1], R. Hagelberg[2], M. Hansroul[2], W. Kienzle[2], A. Lafontaine[1], P. Le Dû[1], J. Lefrançois[5], T. Leray[3], G. Matthiae[2], A. Michelini[2], P. Mine[4], H. Nguyen Ngoc[5], O. Runolfsson[2], P. Siegrist[1], J. Timmermans[2], R. Vanderhaghen[4], J. Valentin[3] and S. Weisz[2]

presented by W. Kienzle

The present report reviews the highlights of the CERN NA3 Experiment on muon pair production by tagged hadron beams (π^-, K^-, $\bar{p}$ and π^+, K^+, p) at 200 (280) GeV/c.

The original aim of the experiment proposed in summer 1974 was "the study of lepton-hadron correlation at large P_t". As a running-in experiment we have measured the inclusive production of muon pairs in order to obtain the structure functions of unstable particles (π, K) by making use of the Drell-Yan process; furthermore as a by-product we have obtained the J/ψ and the upsilon (Υ) resonances, the Υ being observed with a pion beam for the first time.

The following subjects will be discussed:

1. The experimental equipment
   - 1.1 Tagged hadron beam
   - 1.2 Targets and beam dump
   - 1.3 The spectrometer system
   - 1.4 Triggering system
   - 1.5 Acceptance
   - 1.6 Data taking and analysis
2. Results
   - 2.1 Production of Υ resonance(s) by pions
   - 2.2 High-mass continuum and the Drell-Yan mechanism
   - 2.3 Structure function of the pion
3. Summary and conclusions

For details we refer to our publications refs[1-4].

1. THE EXPERIMENTAL EQUIPMENT

The apparatus is shown schematically in fig. 1(a) and photographed in fig. 1(b); this is basically a beam-dump experiment using a tagged hadron beam and a large acceptance magnetic spectrometer for di-muon detection.

1.1 Tagged hadron beam

We have been using an unseparated secondary hadron beam produced by 400 GeV protons on a 50 cm Be target. Particle identification is done by two differential Cerenkov counters (CEDAR) for $K^{\pm}$ and $\bar{p}$, and by two threshold Cerenkov counters for π^+. Beam intensities used in the experiment are in the range from 10^7 to 5×10^7 particles/pulse. At 200 GeV/c the fraction of π^- in the negative beam is about 96%. The fraction of π^+ and K^+ in the positive beam after filtering by a 2 m long CH_2 absorber, was 36% and 4.6%, respectively. Details are shown in table 1.

TABLE 1

CERN SPS 400 GeV protons ($1\text{-}3 \times 10^{12}$ ppp) → 50 cm Be → H8 beam North Area. Beam composition:

(-) beam

Particle	π^-	K^-	$\bar{p}$
Ratio	96.3%	3.1(*)	0.62(*)
Identification	-	C.D.1	C.D.2

2 differential C.D.^{S} = "CEDARS" : 8 PM^S → 8 TDC^S

(+) beam

Particle	π^+	K^+	p
Ratio %	36.0	4.6	59.4
Identification	C1-C2	CD1-CD2	-

2m CH_2 absorber (π^+/p)

2 differential C.D.^{S}

2 threshold C^S(π^+)

The time resolution of the tagging system of $\sigma(t) \approx 0.6$ ns determines the maximum acceptable particle flux due to random background which we limit to about 20% for $\bar{p}$ and K^-.

1.2 Targets and beam dump

A novel feature of this experiment is the simultaneous use of (30 cm) hydrogen and heavy nuclear (platinum) targets, which allows interesting studies of the absolute per (free) nucleon cross section as well as the A-dependence of the Drell-Yan process. Platinum targets, 6 cm in length for the 200 GeV runs and 11 cm for the 280 GeV runs were used. The target was placed 40 cm upstream of a dump consisting of a 1.5 m long block of stainless steel with a heavy (tungsten-uranium) conical plug of ±30 mrad aperture inserted in the centre. The diameter of the Pt target (12 mm) and the tip of the dump (20 mm) were matched to a beam size of σ = 3-4 mm. The target configuration and their separation by reconstructed events are illustrated in fig. 2.

(*) Note that at -150 GeV/c we have now 4.5% and 2% K^- and $\bar{p}$ fractions, respectively; the increase in relative $\bar{p}$ flux has been achieved after optimization of the target length and production angle.

1.3 The spectrometer system (fig. 1)

This has been designed for high acceptance in order to be able to study dileptons in a wide range of kinematic variables. It consists of:

(a) a large superconducting dipole magnet with a vertical field ($\int Bdl$ = 4.0 Tm) in a cylindrically shaped air gap of 1.6 m diameter;

(b) A set of six multiwire proportional chambers (31 planes with a total of about 26 000 wires) ranging in size from 0.6 × 0.6 m^2 to 4.2 × 4.0 m^2;

(c) a muon filter composed of 12 cm of lead and 1.8 m of iron, placed in front of the last triggering hodoscope T3.

The spectrometer is composed of two symmetric telescopes of counters and chambers placed above and below the beam axis. They are covering vertical laboratory angles between ±6 and ±165 mrad. For the mass resolution we refer to fig. 4, below; a typical value is $\sigma \approx 4\%$ and slightly mass dependent.

1.4 Triggering system

A two level trigger was used to minimize the electronics dead-time due to the high particle flux in the chambers. The trigger elements are shown in fig. 3. A "pretrigger" is provided by three planes of counter hodoscopes:

(a) T1 placed at the end face of the beam dump consisting of 12 counters;

(b) T2 which is subdivided into 42 horizontal strips;

(c) T3 situated behind the iron wall, made of 22 horizontal strips.

The "pretrigger" which requires at least two particles in the coincidence T2, T3 and at least one particle in T1, provides a fast strobe for the proportional chambers PC1, PC2, M1 and M2. The pretrigger signal is vetoed by a $\sim$ 1 m^2 halo counter placed upstream of the target. The "trigger" proper acts on the vertical component p^V_T of the transverse momentum of the muons. The p^V_T selection is achieved by two planes of cathode read-out chambers M1 and M2, covering vertical angles from ±30 mrad up to ±165 mrad and an overall azimuthal acceptance of 2/3. The cathodes are printed in 18 separate horizontal bands, each subdivided into 64 cells corresponding to equal intervals of the tangent of the azimuthal angle. The correlation between cells of a given band provides a cut-off in the magnetic deflection angle and thus in p^V_T, which in turn, defines a rough lower cut on the muon pair effective mass. The trigger conditions in the course of the experiment were either $p^V_T > 0.7$ GeV/c for both muons, or $p^V_T > 1$ GeV/c for one muon, without a cut on the other muon.

1.5 Acceptance

The overall acceptance of the apparatus at 200 GeV/c, as determined by the geometry of the detectors and by the p^V_T cut, is shown in fig. 4 as a function of the di-muon fractional momentum x, the transverse momentum P_t, and the dimuon mass (also shown is the dimuon mass resolution). Note that the acceptance value at high masses is better than 30% and almost mass-independent.

1.6 Data taking and analysis

A typical rate of data acquisition is of the order of 30 triggers/pulse or about 200-300 000 events per day written on magnetic tape, or 3 - 5 × 10^6 events per run. The quality of the trigger is illustrated by the percentage of di-muons which is typically 50-60%, with 2-3 J/ψs per pulse or 20 000 J/ψs per day; the J/ψ events serve as a very useful calibration signal in the off-line analysis.

Pattern recognition of both muons is performed in the spectrometer chambers with an overall efficiency of (94 ± 2)%, measured from visual scanning of a sample of reconstructed events. The off-line processing time per event is 20-30 ms. The data reported here represent a total of about 10^7 triggers.

2. RESULTS

The data reported have been taken between September '78 and May '79, with negative and positive beams of 200 (280) GeV/c, the number of events for the different channels are summarized in table 2.

The sensitivity of the experiment is demonstrated by the sample of altogether more than 15 000 Drell-Yan events, and the presence of > 500 000 J/ψs as a byproduct. The amount of π induced Drell-Yan data is subtantially beyond earlier experiments, especially for π^+; the H_2 data are unique but still scarce; the same is true for the highly interesting K^- and $\bar{p}$ events which we hope, however, to increase by an order of magnitude by the end of the year.

TABLE 2

Data (September '78 - May '79)

	Pt target		H_2 target	
	J/ψ	M > 4 GeV	J/ψ	M > 4 GeV
π^- 280 GeV/c	130,000	5700	-	-
⊖ 200 GeV/c	145,000	5916	3000	138
K^-	2,800	119	56	1
$\bar{p}$	1,000	54	17	0
⊕ π^+	108,000	2195	2200	45
K^+	16,000	215	340	2
p	101,000	1304	2200	23

2.1 Resonance production (upsilon)

The overall di-muon mass distribution is shown in fig. 5; apart from a very abundant J/ψ peak(*) at the low mass end we observe here for the first time upsilon production by pions. The Υ : J/ψ cross section ratio is 2 × 10^{-4}. With our mass resolution of $\sigma \approx 4\%$ we are, unfortunately, unable to resolve the Υ substates.

We show here the positive beam data which are particularly well suited for resonance spectroscopy since the physical "background" is 3-4 times less than for π^- events (on nuclear targets) due to the charge

(*) A detailed study of J/ψ production by different incident particles on H_2 and P_t targets has been published elsewhere.[2]

asymmetry of the Drell-Yan process (note that the technical background is entirely negligible). The signal-to-background ratio of the Υ is $\sim$ 4 with 53 ± 12 events above background.

The Υ is more easily observed with π beams since the π/p cross section ratio is as large as 30 which can be understood in the framework of a light quark fusion model of the Υ production mechanism (table 3).

TABLE 3

(a) Υ production by pions

	π^+ 200 GeV/c	π^- 200 GeV/c	π^- 280 GeV/c
$N_{\Upsilon + \Upsilon' + \Upsilon''}$	53 ± 12	55 ± 15	66 ± 20
$B\sigma(\Upsilon's)$ pb/nucleon	1.9 ± 0.6	1.5 ± 0.5	2.4 ± 0.9
$\frac{B\sigma(\Upsilon's)}{B\sigma(J/\psi)}$	$(2.4 \pm 0.6)10^{-4}$	$(1.9 \pm 0.5)10^{-4}$	$(2.2 \pm 0.7)10^{-4}$

(b) Cross section ratios for Υ production

K^+/π^+	0.34 ± 0.23	0.10	light quark fusion model using NA3 structure functions
p/π^+	0.03 ± 0.02	0.05	
π^-/π^+	0.76 ± 0.29	0.83	

The negative beam data are shown in fig. 6 where the Υ signal appears less prominent for reasons as discussed, however with a production cross section compatible with the π^+ data. A comparison of pion and proton cross sections for Υ production as a function of $\tau = M/\sqrt{s}$ is shown in fig. 7. The relative lack of background in the π^+ channel allows a rather clean study of the resonance such as for example the x distribution shown in fig. 8; the asymmetric x distribution with $\langle x \rangle \approx 0.2$ is a consequence of the difference between π and nucleon structure. We have also examined the Υ decay angular distribution (not shown here) and find it compatible with flat, in contrast to the adjacent Drell-Yan continuum events (see next paragraph).

Finally the various parameters of our Υ results have been summarized in table 3.

2.2 High-mass continuum and the Drell-Yan process

The original aim of this experiment has been a measurement of the quark structure of unstable hadrons (π, K) by use of the Drell-Yan process. The Drell-Yan mechanism provides a simple model of lepton-pair production in hadronic reactions where a quark and a antiquark of the beam and target particles annihilate electromagnetically into a virtual photon with subsequent decay into e^+e^- or $\mu^+\mu^-$ pair.

Measurement of the lepton pair's invariant mass M and fractional momentum x uniquely determine the x_1 and x_2 of the annihilation quarks in the projectile and target particle; thus their structure functions can be extracted.

DRELL-YAN MECHANISM

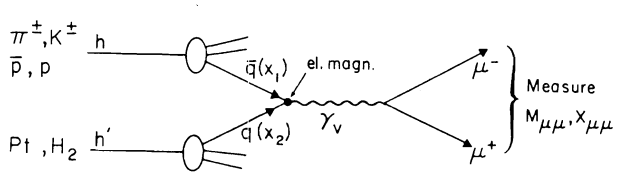

We measure:

$$M^2_{\mu\mu} = x_1 x_2 s$$

$$X_{\mu\mu} = x_1 - x_2 = \frac{2P_L^*}{\sqrt{s}} \quad \left| \begin{array}{l} \text{calculate } x_1,\ x_2,\ d^3\sigma/dM\ dx_1 dx_2 \\ (p_t \text{ neglected}) \end{array} \right.$$

Extract structure functions $f(x_1)$, $f(x_2)$:

$$\frac{d^2\sigma}{dx_1\,dx_2} = \frac{4\pi\alpha^2}{3s}\,\frac{1}{3}\,\Sigma_i\,\frac{Q_i^2}{x_1^2 x_2^2}\,[f_i^h(x_1)\,f_{\bar{i}}^{h'}(x_2) + f_{\bar{i}}^h(x_1)\,f_i^{h'}(x_2)]$$

$$\frac{d^2\sigma}{dMdx} = \frac{8\pi\alpha^2}{3M^3}\,\frac{1}{3}\,\Sigma_i\,\frac{Q_i^2}{x_1 + x_2}\,[f_i^h(x_1)\,f_{\bar{i}}^{h'}(x_2) + f_{\bar{i}}^h(x_1)\,f_i^{h'}(x_2)]\ .$$

In the present experiment we have been proceeding in two steps:

(a) Experimentally testing the D.Y model.
(b) Application to the pion structure function.

Concerning the first point there are a number of specific features of di-muon production which must be satisfied in the high-mass continuum if the D.Y. model is correct:

(a) A-dependence: incoherence of $\bar{q}q$ annihilation → cross section $\propto A$.

(b) Charge asymmetry

$$\frac{\sigma(\pi^+ N)}{\sigma(\pi^- N)} \propto \frac{\bar{d}d}{\bar{u}u}\ (\text{for large } \tau) \begin{array}{l} \to 1/4 \quad I = 0 \quad \text{target} \\ \to 1/8 \quad H_2 \quad\quad (\text{assuming } u = 2d) \end{array}$$

(c) Decay angular distribution: $\gamma_v(1^-) \to 1 + \lambda\cos^2\theta \to \lambda = 1$.

(d) Scaling: $M^3 d\sigma/dM = f(M/\sqrt{s})$.

(e) Absolute cross section: predictable for reactions with known structure functions.

2.2.1 A-Dependence of the D.Y. cross section

Due to the incoherent nature of the quark annihilation process in the D.Y. model, the target acts like an assembly of free quarks, the cross section is therefore expected to be linear in A, i.e. $\sigma_{D.Y.} \sim A^{\alpha}$ with $\alpha = 1$, contrary to purely hadronic reactions.

In our analysis we compare the H_2 with the Pt data (table 2). We take advantage of having both π^- and π^+ data: by using the cross section difference $\sigma = \sigma(\pi^-) - \sigma(\pi^+)$ we eliminate sea effects.

We measure

$$A\frac{\sigma(H)}{\sigma(Pt)} = 1.51 \pm 0.28$$

$$= A^{1-\alpha} R(x_2) \text{ where}$$

$$R(x_2) = \frac{4u - d}{u + 2d} = \frac{\sigma(\pi^- - \pi^+) \text{ on } H_2}{\sigma(\pi^- - \pi^+) \text{ on Pt}}$$

We have used two relations u vs. d:

(a) $u = 2d \rightarrow R(x_2) = 7/4 = 1.75$ or

(b) $2d/u = 1.125(1 - x) \rightarrow R(x_2) = 1.8$ at $\langle x_2 \rangle^{\text{expt.}} = 0.15$

thus

$$A^{\alpha-1} = \frac{1.80}{1.51} \rightarrow \alpha_{D.Y.} = \underline{1.03 \pm 0.03}$$

Other experiments find:

$\alpha = 1.02 \pm 0.02$ for p on Be, Cu, Pt (CFS Collaboration, L. Lederman, Tokyo Conf.[9]).

$\alpha = 1.12 \pm 0.05$ for π^- on Cu, C, W (CIP Collaboration, J. Pilcher et al.[10]).

The latter may have to be reconsidered, however, since it also leads to non-scaling of the CIP data, as discussed below. Notice that CIP and NA3 agree as far as the per-nucleus cross section is concerned.

2.2.2 Charge asymmetry

The electromagnetic nature of the D.Y. process implies that differently charged quarks produce different annihilation cross sections. This leads to a charge-asymmetry in contrast to hadronic processes. Example:

$$\left.\begin{aligned} &\frac{\pi^+ p}{\pi^- p} = \frac{\bar{d}d}{2\,\bar{u}u} \rightarrow \frac{1/9}{2x4/9} = \frac{1/8 \text{ on}}{H_2} \\ &\frac{\pi^+ \text{ nucleon}}{\pi^- \text{ nucleon}} \rightarrow 1/4 \text{ for a } I = 0 \text{ target} \end{aligned}\right\} \begin{array}{l}\text{in the limit of } M/\sqrt{s} \rightarrow 1, \\ \text{and in the approximation} \\ \text{that the sea quarks are} \\ \text{neglected and that the x} \\ \text{distributions of u and d} \\ \text{are the same.}\end{array}$$

The exact asymptotic value depends on the I-spin composition of the target as well as on the structure functions.

The experimental data closely reproduce this most striking prediction of the D.Y. model as shown in fig. 9.

2.2.3 Angular distribution

A $1 + \lambda\cos^2\theta$ distribution with $\lambda = 1$ (for instance in the Gottfried-Jackson frame) is expected because of the intermediate photon γ_v. The experimental data agree within errors, as seen in fig. 10.

Notice that in fig. 9 we have limited the transverse momentum to $P_t \lesssim 1$ GeV/c; this is because at large P_t and/or large x, the picture becomes more complicated since $\sin^2\theta$ terms are expected[10].

2.2.4 Scaling

Scaling in the form $M^3 d\sigma/dM = f(M/\sqrt{s})$ is an inherent feature of the D.Y. process. Our data at 200 and 280 GeV/c (fig. 10) support this hypothesis, as well as the pN data of ref. 9 at higher energies. The data of Anderson et al.[10] are in apparent disagreement (factor ~ 2 below fig. 11); this is however related to their extraction of the "per nucleon" cross section through their non-linear $A^{1.12}$ dependence, as mentioned above see 2.2.1. Notice that the $\log Q^2$ dependence observed for instance in deep inelastic lepton scattering is too small to be detected in our data (5% effect in our range of Q^2)

2.2.5 Absolute value of the D.Y. cross section

Tests (a)-(d) discussed above are well described by the D.Y. process and one would conclude up to here that the model is essentially correct. There are however, two experimental facts to complicate the situation:

(a) Large P_t events, i.e. about half of the di-muons have $P_t \gtrsim 1$ GeV/c. There are two comments to made here, first, the D.Y. model assumes $P_t = 0$ therefore whatever P_t distribution found experimentally cannot be regarded as a test of the model. Secondly the fact that a substantial fraction of the events is above what one can reasonably assume as "primordial" P_t of the quarks (i.e. their "Fermimotion" in the nucleon, for instance 0.3 - 0.7 GeV/c) goes beyond the simple quark model anyhow; additional mechanisms are needed.

(b) The absolute cross section of the D.Y. process is determined as

$$\frac{d^2\sigma}{dx_1 dx_2} = \frac{4\pi\alpha^2}{3s} \cdot \frac{1}{3} \cdot \sum_i \frac{Q^2 i}{x_1^2 x_2^2} \{f_i(x_1)\, \bar{f}_i(x_2) + \bar{f}_i(x_1)\, f_i(x_2)\} \qquad (1)$$

where the Q_i are the quarks fractional charges and $f_i(x_1)$, $\bar{f}_i(x_2)$ are the effective structure functions of the projectile and target particles respectively. The so-called "naive" model does therefore not contain any free parameter and the absolute value of the cross section is predicted exactly for reactions where both the projectile and target particle (i.e. their structure function) are known, for instance for $p(\bar{p})N$ known from deep inelastic lepton scattering experiments.

The present experimental data allow us to check this prediction in quantitative detail. For the first time, deviations from the simple model D.Y. have been found. If we express the ratio of measured over the expected D.Y. cross section by a scale factor K defined as

$$\sigma(D.Y.)_{exp'tl} = K\sigma(D.Y.)_{theory}$$

we find that $K \approx 2$ from four independent reaction channels at 200 GeV/c: pN, $\bar{p}N$, $\pi^- N$ (for P_t), and $\pi^- H_2$.

The values of the K factor in the four different channels are summarised in table 4.

TABLE 4

Summary $\sigma_{D.Y.}^{exp.}/\sigma_{D.Y.}^{theor.} = K$

Reaction	PN	$\bar{p}N$	$\pi^- N$	$\pi^+ N$	$\pi^- H_2$	$\pi^- - \pi^+$
K	2.2	2.4 ± 0.4*) (44 events)	2.2	2.4	2.4 ± 0.2 (138 events)	2.2

using CDHS nucleon

$K = 2.3$ (± 0.5 systematic error(*))

The following specific remarks should be made:

2.2,5.1 pN data

(a) The nucleon structure function from D.Y.

The practical use of the D.Y. mechanism to measure structure functions of unstable hadrons can be tested directly by comparing the proton structure function obtained from D.Y. data with that from deep inelastic lepton scattering (at equal $Q^2 = -M^2$). NA3 is in a good position to perform such a study because of its large acceptance. This comparison is essential in order to justify the use of structure functions from deep inelastic lepton scattering to predict the "theoretical" D.Y. cross section.

Our pN data were obtained at 200 GeV/c with a mixed positive beam (table 1) incident on a 6 cm platinum target. There are 1300 proton induced di-muon events in the mass region above 4 GeV useful for a D.Y. type analysis; their mass distribution is shown in fig. 12.

The data have been analysed as follows:

(i) Parametrization of the proton

valence
$$\begin{cases} u^p = A_{\alpha\beta}^{\ u}\, x^\alpha (1-x)^\beta \quad \text{with } \int \frac{u^p}{x}\,dx = 2 \\ d^p = A_{\alpha\beta}^{\ d}\, x^\alpha (1-x)^{\beta+1} \text{ with } \int \frac{d^p}{x}\,dx = 1 \end{cases}$$

sea
$$\begin{cases} \bar{u} = \bar{d} = A_s (1-x)^{\beta_s} \\ \bar{s} = 1/4(\bar{u} + \bar{d}) \leftarrow \text{CDHS result}^{11} \end{cases}$$

$$\begin{cases} \alpha, \beta, \beta_s \text{ free parameters} \\ \langle G\rangle: \text{ average fractional momentum carried by gluons: fixed} \\ A_s \text{ determined by } 5A_s/(\beta_s+1) = 1 - \langle G\rangle - \langle u\rangle - \langle d\rangle. \end{cases}$$

(ii) Results of the fit

The parameters of the proton structure function from the D.Y. data are compared to the D.I.S. data (CDHS) in table 5.

(*) Statistical errors are indicated for the channels with low event rates. The overall systematic error of ± 0.5 takes into account the uncertainties in beam normalisation, acceptance, and detection efficiencies.

TABLE 5

Parameters of the proton structure

	NA3	CDHS(Q^2 = 20)
$\langle G\rangle$	0.5 (fixed)	0.5
α_u	0.52 ± 0.2	0.51 ± 0.02
β_u	3.2 ± 0.4	2.8 ± 0.1
$\langle u + d\rangle$	32%	34%
β_s	9.4 ± 1.0	8.1 ± 0.7
A_s	0.37	0.27
$\langle$sea$\rangle$	18%	15%

Fig. 13 shows the agreement between our data and the CDHS nucleon parametrisation.

Conclusion: - first determination of the nucleon structure using μ pairs,
- good agreement between D.Y. and DIS determination of the nucleon structure.

(b) The absolute cross section

Since our analysis has shown that the D.Y. nucleon structure parameters agree with CDHS at equal Q^2, we can now use the latter as input to compute the D.Y. cross section and derive K by comparison with the experiment; this leads to the pN value of K in table 4.

2.2.5.2 $\bar{p}N$ data

The weak point in determining K from pN data is the necessity of fixing the percentage of sea-quarks to the value found in the lepton scattering experiments (e.g. CDHS data), since one cannot, in principle distinguish in a D.Y. experiment between, say K = 2 and a twice larger sea.

The cleanest experimental way of obtaining K is using antiprotons since in $\bar{p}N$ reactions the valence-sea terms contribute only < 15% to the D.Y. cross section.

The $\bar{p}$ experiment is however difficult and we have collected so far only 44 D.Y. events with M > 4 GeV, at 200 GeV/c on Pt; they are shown in fig. 14.

We obtain $K(\bar{p}N) = 2.4$ (± 0.4 statistical error).

This result would mean that the result K(pN) (last paragraph) cannot be due to an increased percentage of sea in the D.Y. reaction, as compared to lepton scattering.

2.2.5.3 π data

Pion data are in principle similar to $\bar{p}$ as to the dominance of the valence-valence term; however the definition of K is less direct since the π structure function cannot be determined independently by lepton scattering. On the other hand our analysis in ref.[4] shows that the π structure function is insensitive to details of the target nucleon since x_1 and x_2 are almost uncorrelated; we use

$F_\pi^{val}(x_1) \sim x_1^{0.4}\,(1-x_1)^{0.9}$ (details see sect. 2.3.1).

(a) $\pi^{\pm}$ - Pt data

We refer to ref.[4] for a detailed description of the method of analysis. The data are shown in fig. 15 for π^+ and π^-, giving K = 2.4 and 2.2 respectively.

We have also analyzed $\pi^- - \pi^+$ difference which has the advantage that sea effects and possible contributions from hadronic sources of di-muons are eliminated; this analysis leads to K = 2.2.

(b) π^--H_2 data

A more direct way of measuring K with π^s is to use a H_2 target. This has the advantage that A = 1 and therefore no A^α dependence is involved. From our 138 $\pi^- H_2$ events with M > 4 GeV we obtained K = 2.4. The data are shown in fig. 16. For the $\pi^- - \pi^+$ data (93 events) we get K = 2.2 ± 0.2.

We also note that CIP Collaboration found $K \approx 1$ for π^-W at 225 GeV/c[10]; this result is probably related to their $A^\alpha = A^{1.12}$ which leads to a factor of 2 in the "per nucleon" cross section for A = 195 of the Pt nucleus. Assuming linear A-dependence the CIP experiment is compatible with $K \approx 2$.

The Goliath Collaboration π^-Be at 150 GeV/c[12] finds $K \approx 3$ assuming again a linear A dependence.

Conclusion concerning the absolute D.Y. cross section

The overall conclusion concerning the absolute experimental D.Y. cross section is that the latter is larger than expected from the so-called "naive" D.Y. model (using deep inelastic nucleon structure functions as input) by a factor of about two.

An effect of this size has been predicted by theory as being due to QCD (gluestrahlung) corrections to the normal D.Y. formula (for a review see ref.[13]).

Di-muon production by antiprotons is the ideal test of QCD corrections to D.Y. NA3 is now concentrating on this channel with the aim of gaining about an order of magnitude on our present data.

A more detailed discussion of the K factor in the different reaction channels will be published elsewhere (ref.[14]).

2.3.1 Structure function of the pion

Pion - Nucleon data at 200 GeV/c (see fig. 17).

(a) Definitions

$$\frac{d^2\sigma}{dx_1 dx_2} = \left(\frac{4\pi\alpha^2}{3s}\right)\frac{1}{3}\frac{1}{x_1^2 x_2^2}\left[V_\pi(x_1)\,G(x_2) + S_\pi(x_1)\,H(x_2)\right]$$

(V_π: beam, G: target; S_π: beam, H: target)

Valence:

π^- : $v_\pi(x_1) \equiv u_v^{\pi^-} = d_v^{\pi^-} = u_v^{\pi^+} = \bar{d}_v^{\pi^+}$

nucl.: $\begin{cases} u(x_2) \equiv u_v^p = d_v^n \\ d(x_2) \equiv d_v^p = u_v^n \end{cases}$

sea: $S_\pi(x_1)$, $S_n(x_2)$

Normalisation of quark number:

$$\int \frac{v_\pi(x_1)}{x_1}\,dx_1 = 1, \quad \int \frac{u(x_2)}{x_2}\,dx_2 = 2, \quad \int \frac{d(x_2)}{x_2}\,dx_2 = 1.$$

Pt target ($I \neq 0$) : Z/A = 0.4

$$G(x_2) = 1/9\ (1.6u + 2.4d + 5S_n)\ \pi^-$$

$$= 1/9\ (0.6u + 0.4d + 5S_n)\ \pi^+$$

$$H(x_2) = 1/9\ (2.2u + 2.8d + 12S_n)\ \pi^+, \pi^-$$

(b) Parametrization of the π, N structure functions

Nucleon	Pion
$u(x_2) = A_u\, x_2^{\alpha_u}(1 - x_2)^{\beta_u}$	$V_\pi(x_1) = A_\pi x_1^{\alpha_\pi}(1 - x_1)^{\beta_\pi}$
$d(x_2) = A_d\, x_2^{\alpha_u}(1 - x_2)^{\beta_u + 1}$	$S_\pi(x_1) = B_\pi(1 - x_1)^{\beta_\pi s}$
$S(x_2) : \bar{u} = \bar{d} = A_s(1 - x_2)^{\beta_u s} = \bar{s}$	

(c) Results

Nucleon		Pion	
CDHS = input ($Q^2 = 20$)[11]			
$\alpha_n = 0.51 \pm 0.02$	mom. fractions:	$\alpha_\pi = 0.37 \pm 0.02$	mom. fractions
$\beta_n = 2.8 \pm 0.1$	val. = 34%	$\beta_\pi = 0.92 \pm 0.03$	val. = 32%
$\beta_n^s = 8.1 \pm 0.1$	sea = 15% symmetric	$\beta_\pi^s = 5$ fixed	sea = 13%

Conclusion: $F_\pi^{val.} \sim x^{0.4\pm0.1}(1 - x)^{0.9\pm0.1}$ (fig. 18)

Note that this result is independent of details of the target structure functions.

3. SUMMARY AND CONCLUSIONS

(a) Upsilon: first evidence for Υ production by π^s

$\sigma(\pi) \gtrsim 30\sigma(p)$ and $B\sigma(\Upsilon)/B\sigma(\psi) \approx 2 \times 10^{-4}$

(b) Muon pair continuum

"Drell-Yan mechanism":
- A-dependence
- charge asymmetry
- angular distribution
- scaling

} classical Drell-Yan model O.K.

But: absolute experimental cross section > naive D.Y. model predictions by factor K = 2.3 (±0.5)

(c) π structure function

$F_\pi^{val.} \sim x^{0.4\pm0.1}(1 - x)^{0.9\pm0.1}$

REFERENCES

1 J. Badier et al., First evidence for upsilon production by pions, Phys. Lett. 86B (1979) 98.

2 J. Badier et al., Di-muon resonance production from 200 and 280 GeV/c tagged hadron beams, Int. High Energy Physics Conf. Geneva 1979.

3 J. Badier et al., Muon pair production at masses above 4 GeV (Drell-Yan Continuum), Int. High Energy Phys. Conf, Geneva 1979.

4 J. Badier et al., Experimental determination of the pion and nucleon structure functions by measuring high-mass muon pairs, Int. High Energy Conf., Geneva 1979.

5 J.K. Yoh et al., Phys. Rev. Lett. 41 (1978) 684.

6 I. Mannelli, Electron pair production at the ISR, Proc. 19th Int. Conf. on High Energy Physics (Tokyo 1978), (Physical Society of Japan, Tokyo, 1979) 189.

7 A.L.S. Angelis et al., A measurement of the production of massive e^+e^- pairs in p-p collision at $\sqrt{s}$ = 63 GeV, presented at the EPS Int. Conf. on High Energy Physics, Geneva 1979.

8 D. Antreasyan et al., Dimuon spectra from 62 GeV proton collisions, presented at the EPS Int. Conf. on High Energy Physics, Geneva 1979.

9 L.M. Lederman, Dilepton production in hadron collision, Proceedings of the 19th Int. Conf. on High Energy Physics, Tokyo 1978.

10 J. Pilcher, Review of di-muon production in hadron collision, this conference.

11 For a review of the results of the CDHS Collaboration see for instance: A. Para, Recent measurements of nucleon structure functions from neutrino scattering, this conference.

12 R. Barate et al., Production of high-mass muon pairs in π^-Be collision at 150 and 175 GeV/c, submitted to Phys. Rev. Lett. and CERN/EP 79-87.

13 G. Altarelli, Lepton pair production, presented at the EPS Int. Conf. on High Energy Physics, Geneva 1979.

14 J. Badier et al., The absolute cross section of di-muon production in hadron collision in the Drell-Yan continuum, submitted to Phys. Letters.

DISCUSSION

Discussion combined in James Pilcher's paper, the next paper in sequence.

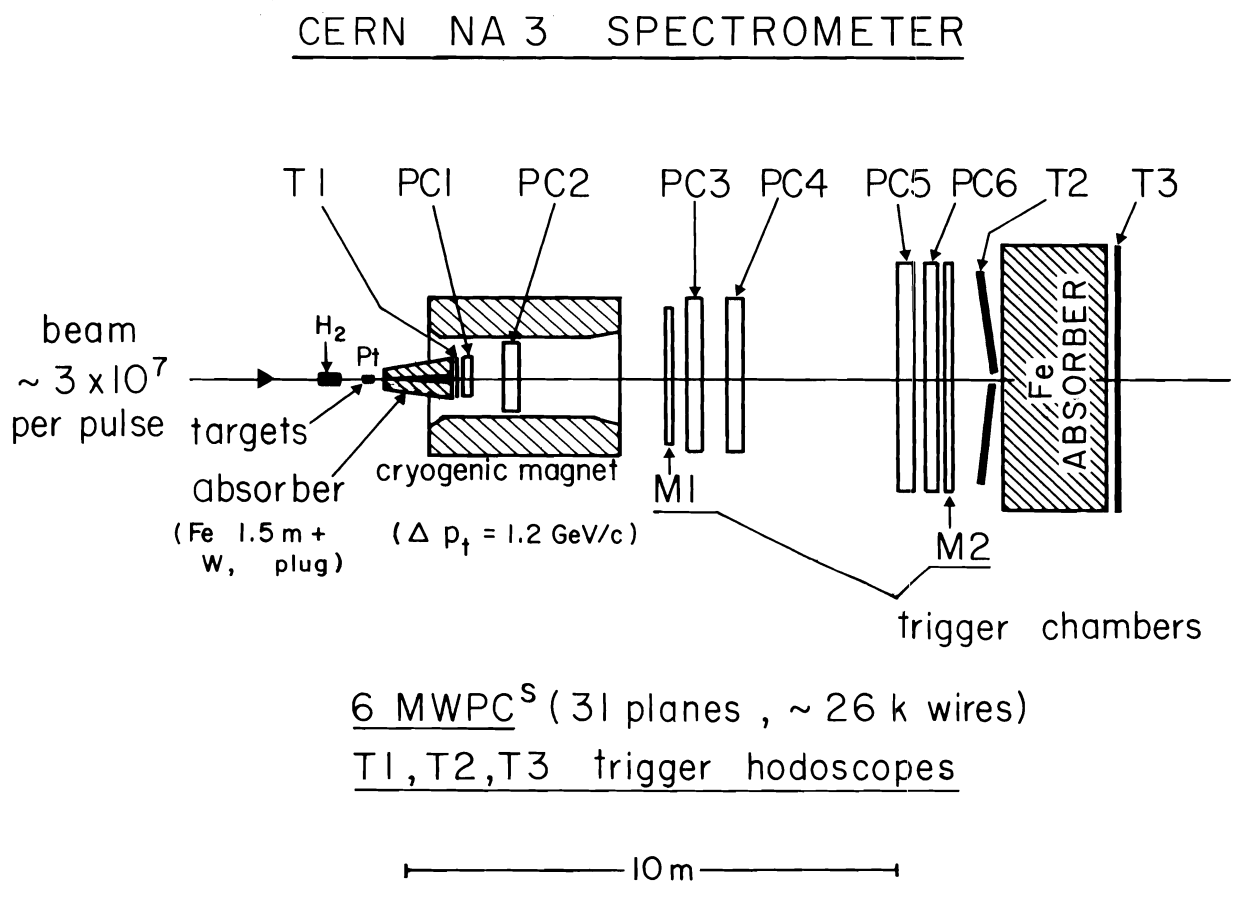

Fig. 1 (a) Layout of the NA3 spectrometer (schematically)

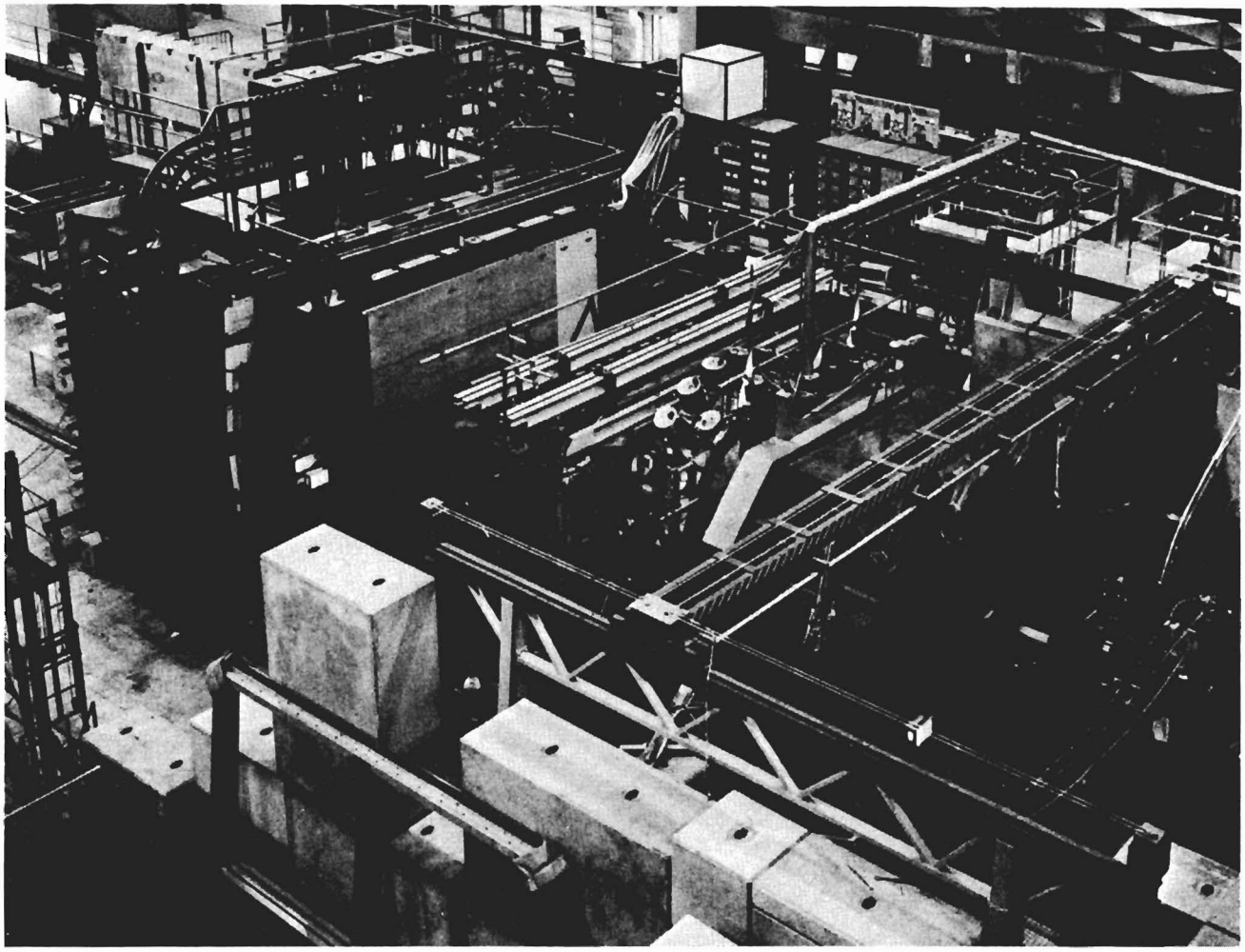

Fig. 1(b). Layout of the NA3 spectrometer (photograph).

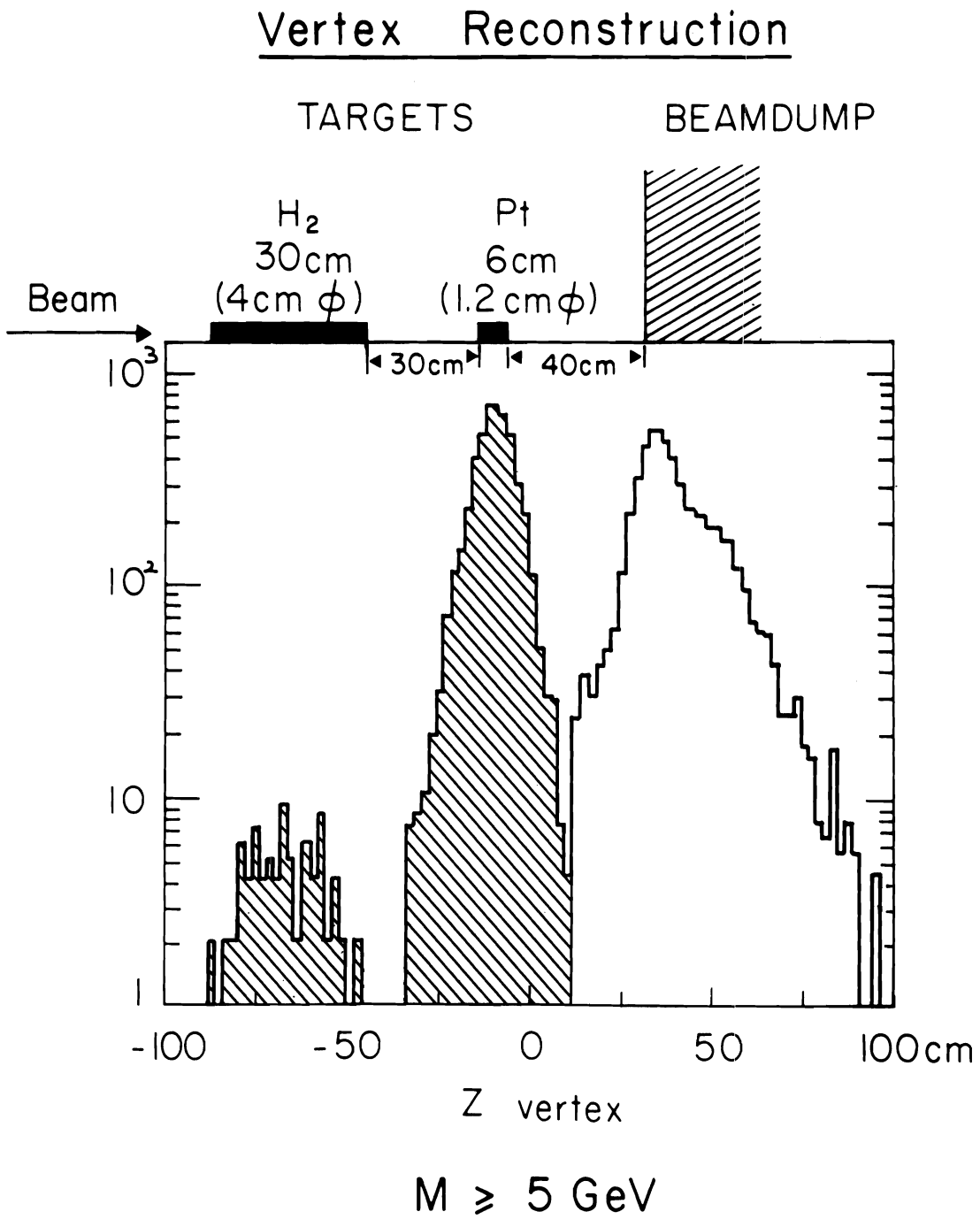

Fig. 2 Vertex reconstruction : separation of the targets from the beam dump.

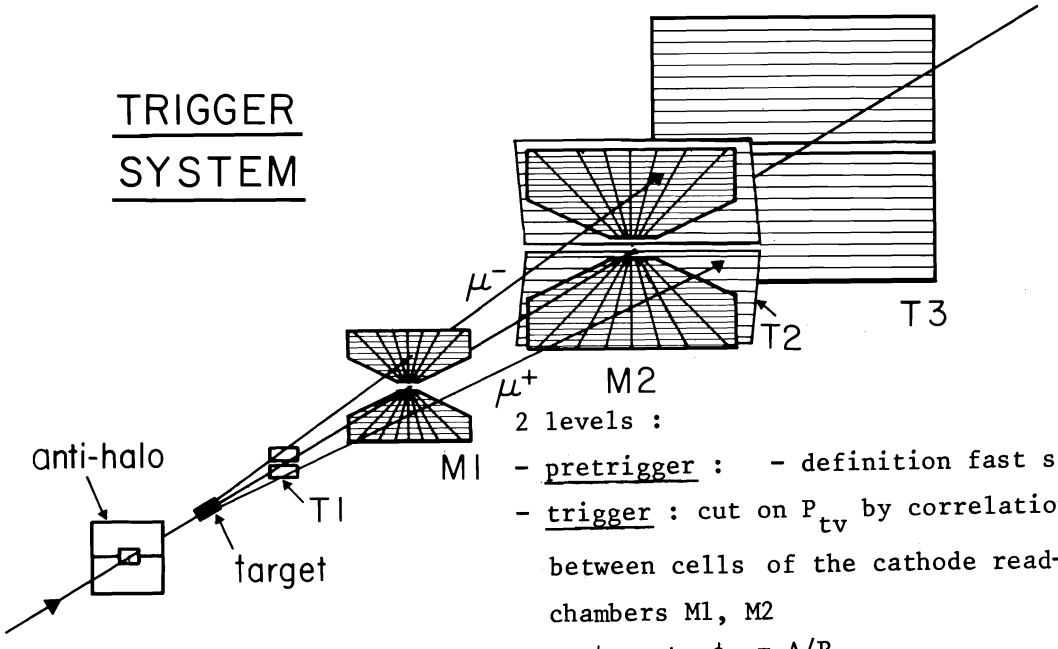

2 levels :

- pretrigger : - definition fast strobe
- trigger : cut on P_{tv} by correlations between cells of the cathode read-out chambers M1, M2

$tg\ \phi_1 - tg\ \phi_2 = A/P_{tv}$

rough cut on $M_{\mu\mu} > 2$ GeV

- one muon : $P_{tv} > 1$ GeV/c
- both muons : $P_{tv} > 0.7$ GeV/c

Fig. 3. Trigger System.

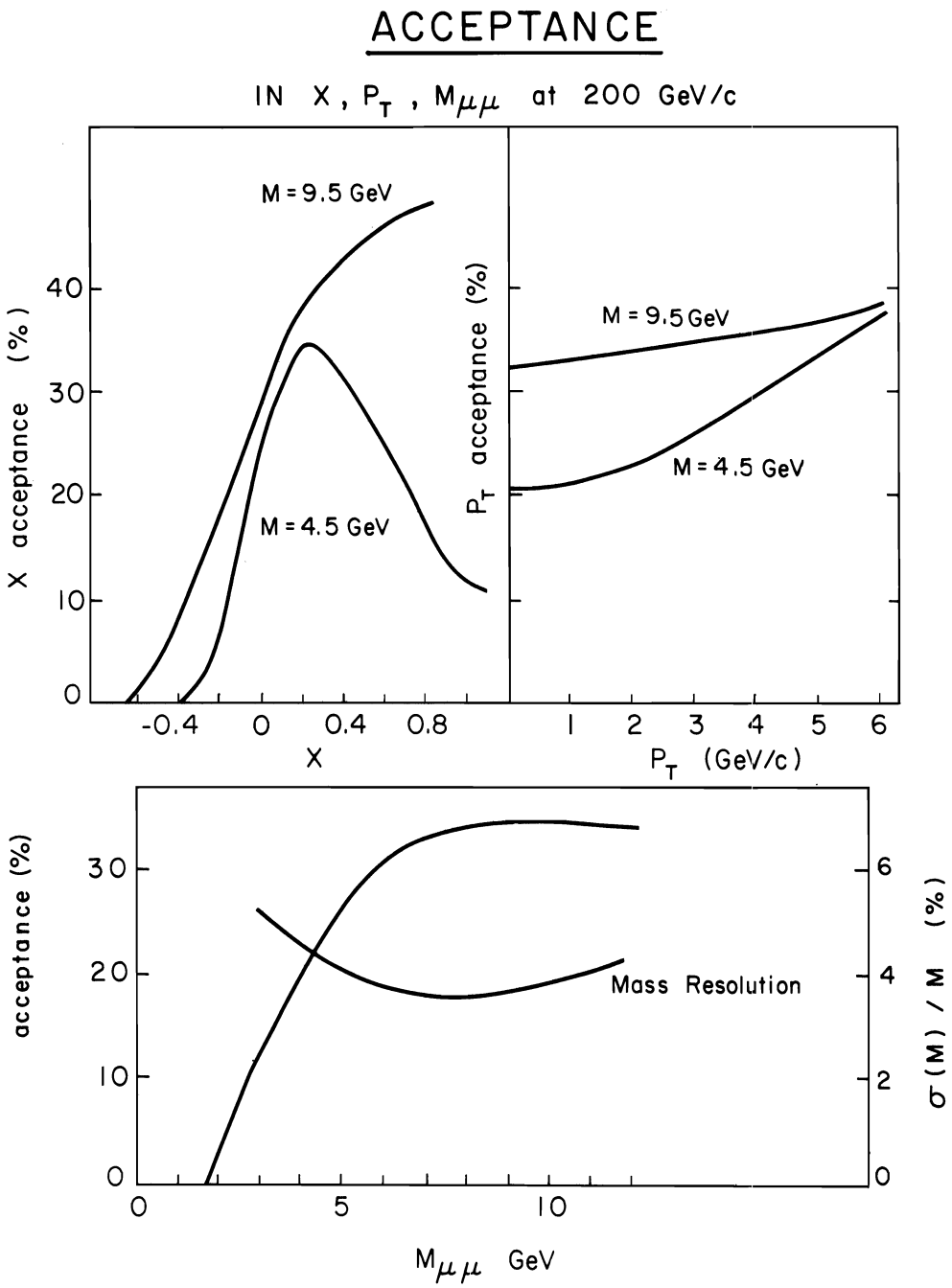

Fig. 4 Acceptance vs. x, Pt and M of the di-muons.

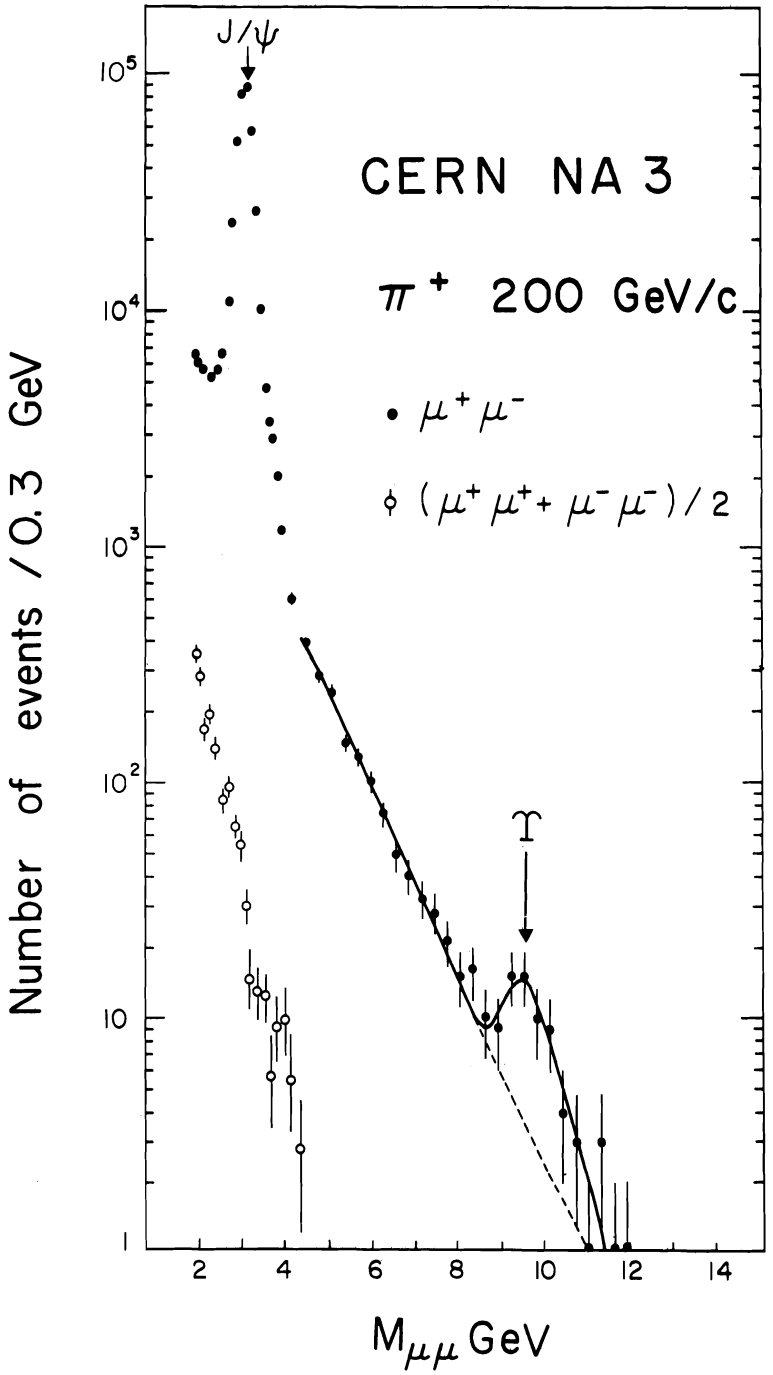

Fig. 5 Di-muon mass distribution for π^+ at 200 GeV/c.

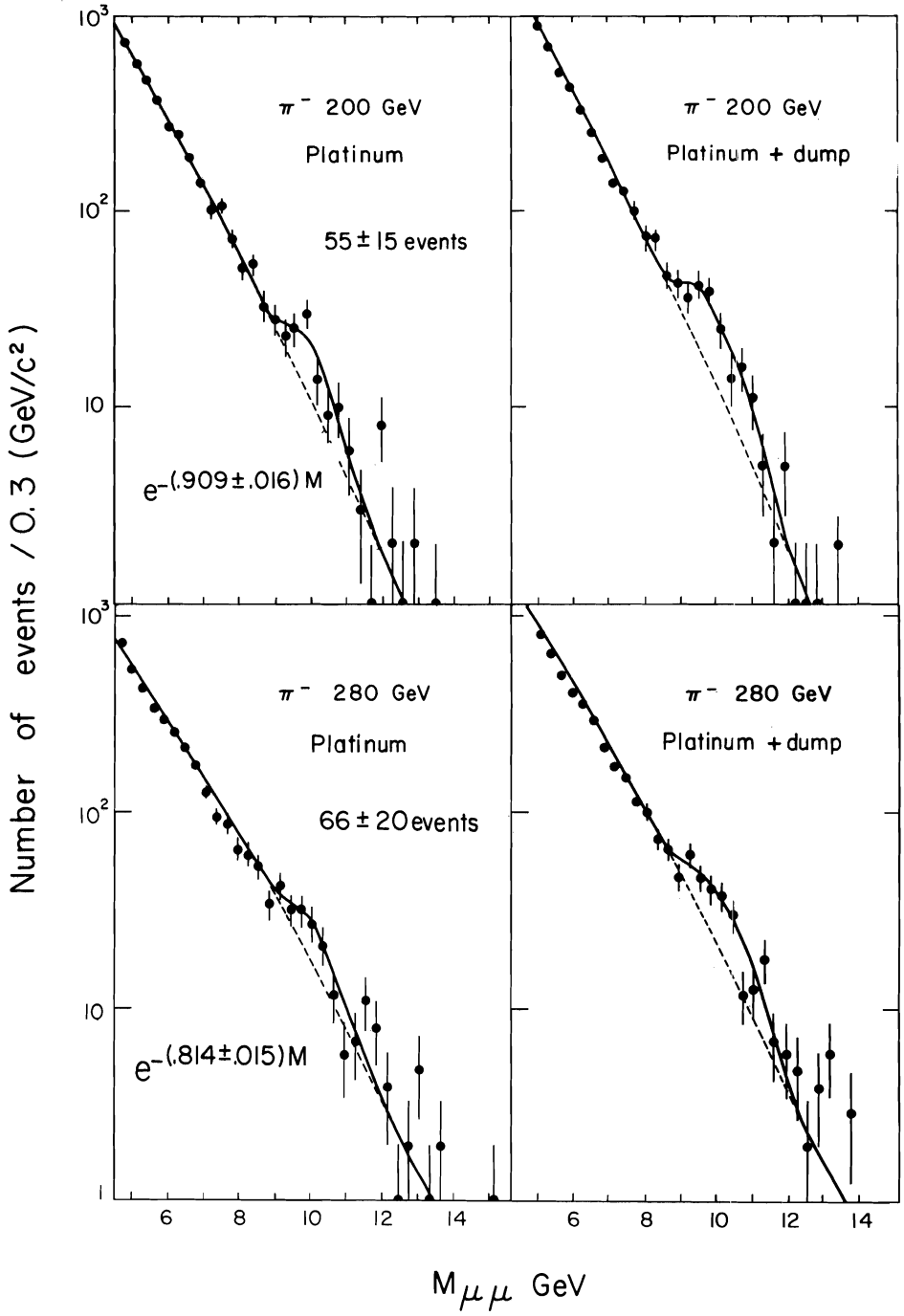

Fig. 6 Di-muon mass distribution for π^- at 200 and 280 GeV/c.

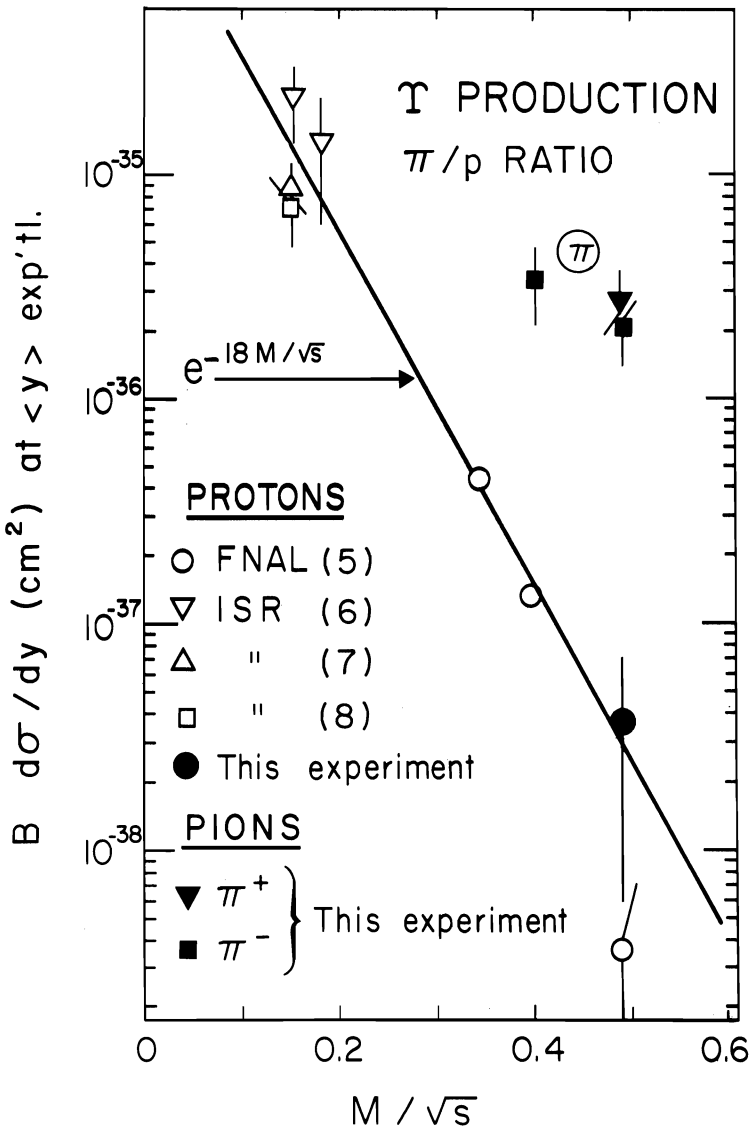

Fig. 7 Cross section comparison between protons and pions for T production.

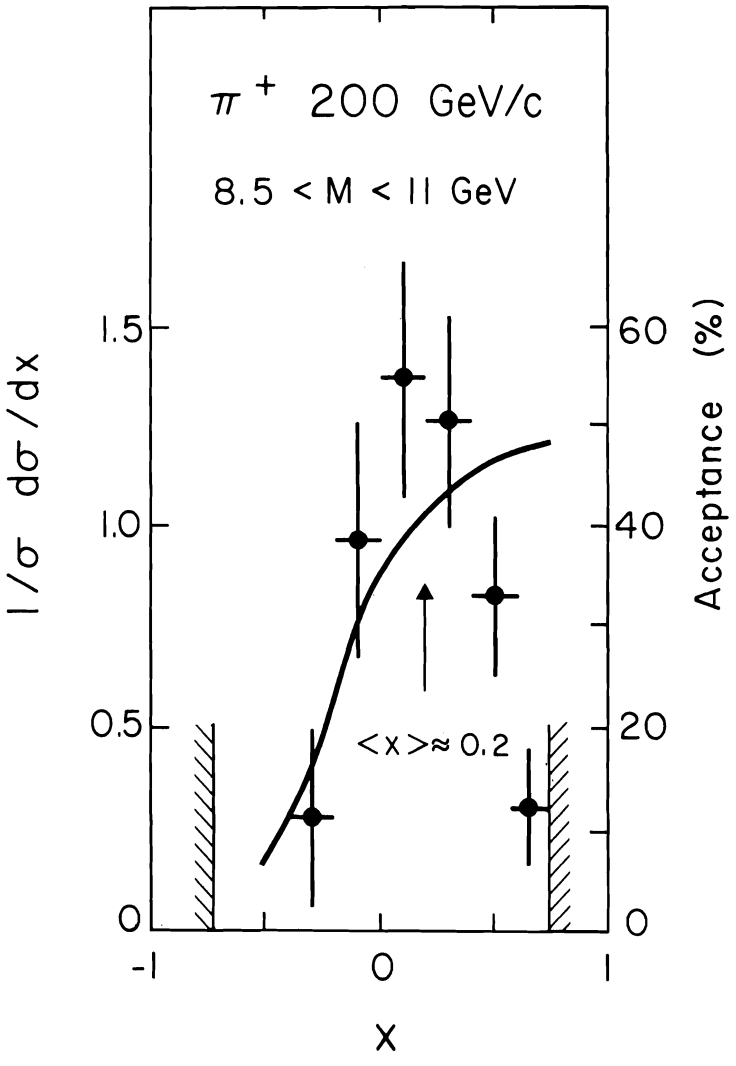

Fig. 8 X - distibution for T events.

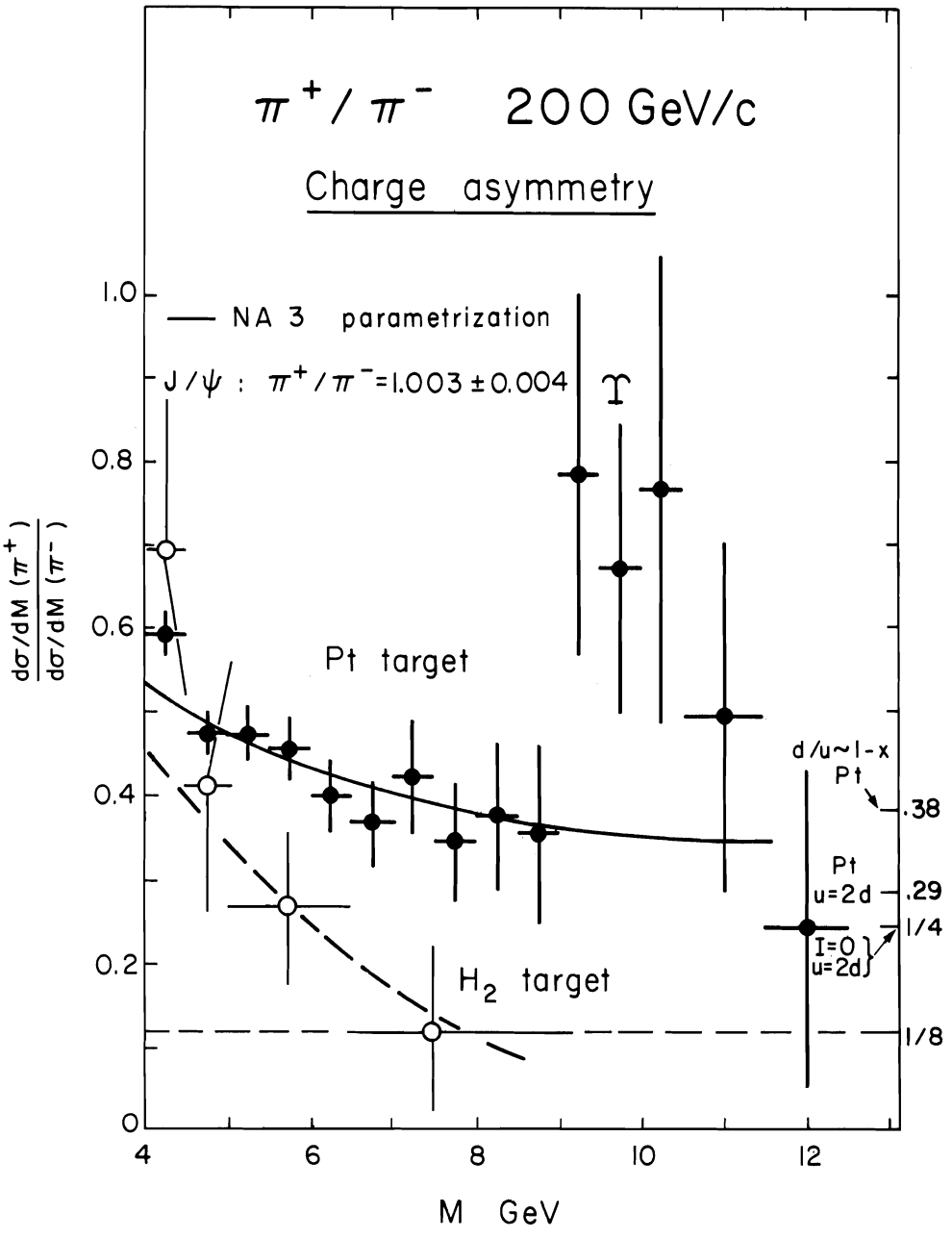

Fig. 9 Charge asymmetry of the D.Y. process

Decay angular distribution

$1 + \lambda \cos^2 \theta^*$

Gottfried - Jackson : $\lambda = 0.80 \pm 0.17$

Collins - Soper : $\lambda = 0.85 \pm 0.17$

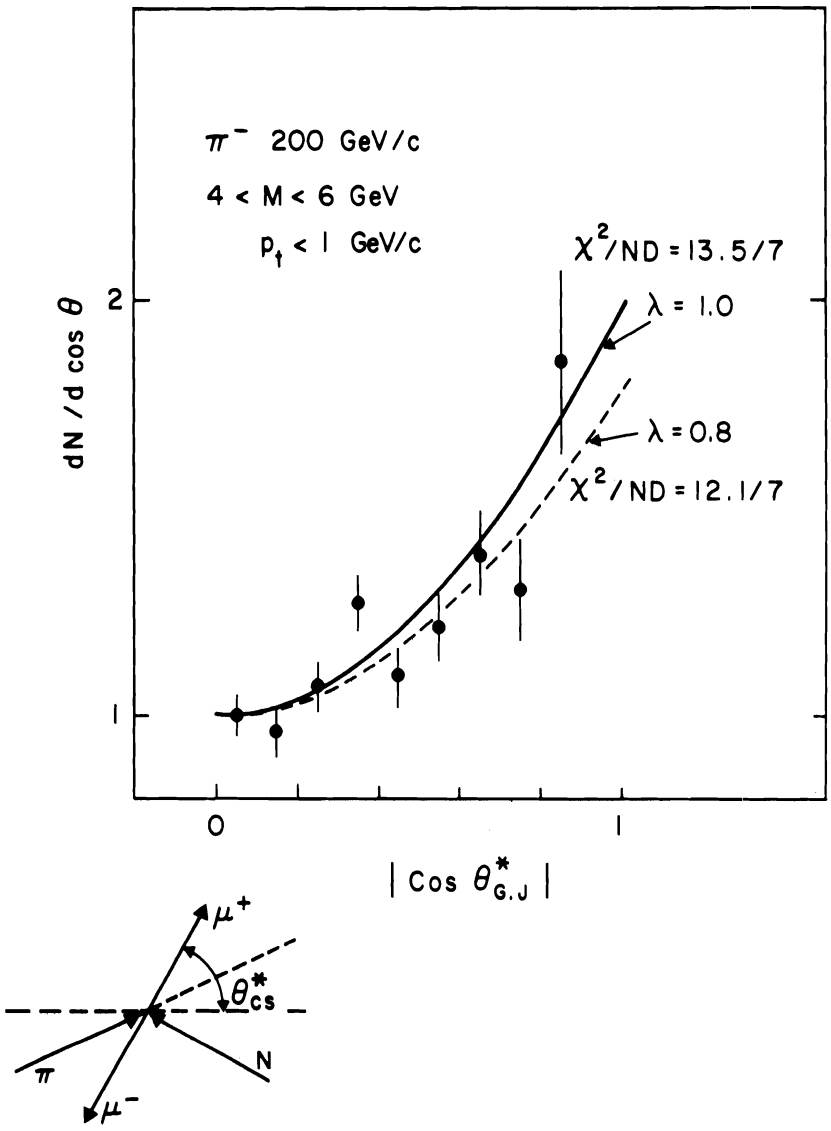

Fig. 10 Decay angular distribution.

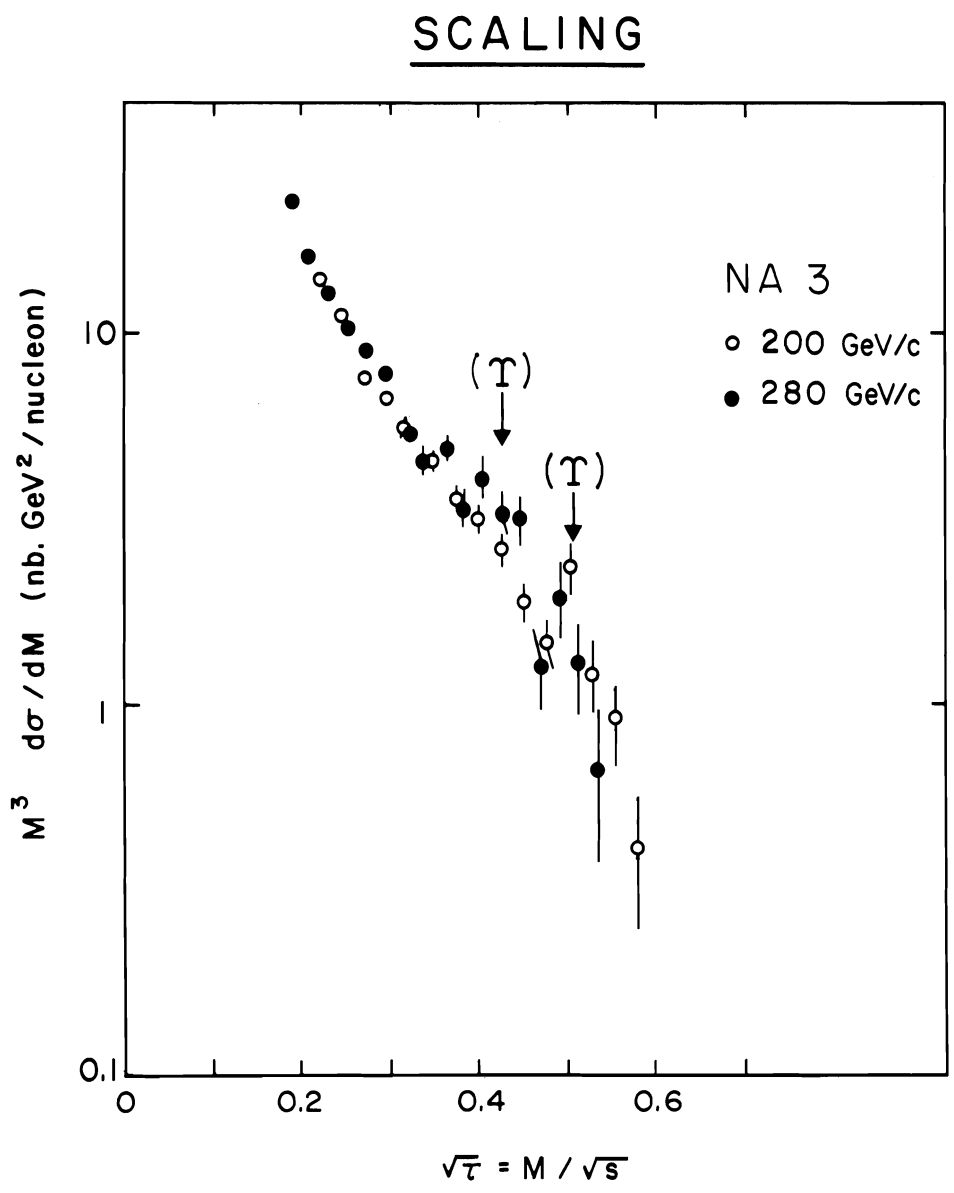

Fig. 11 Scaling of $M^3 d\sigma/dM$.

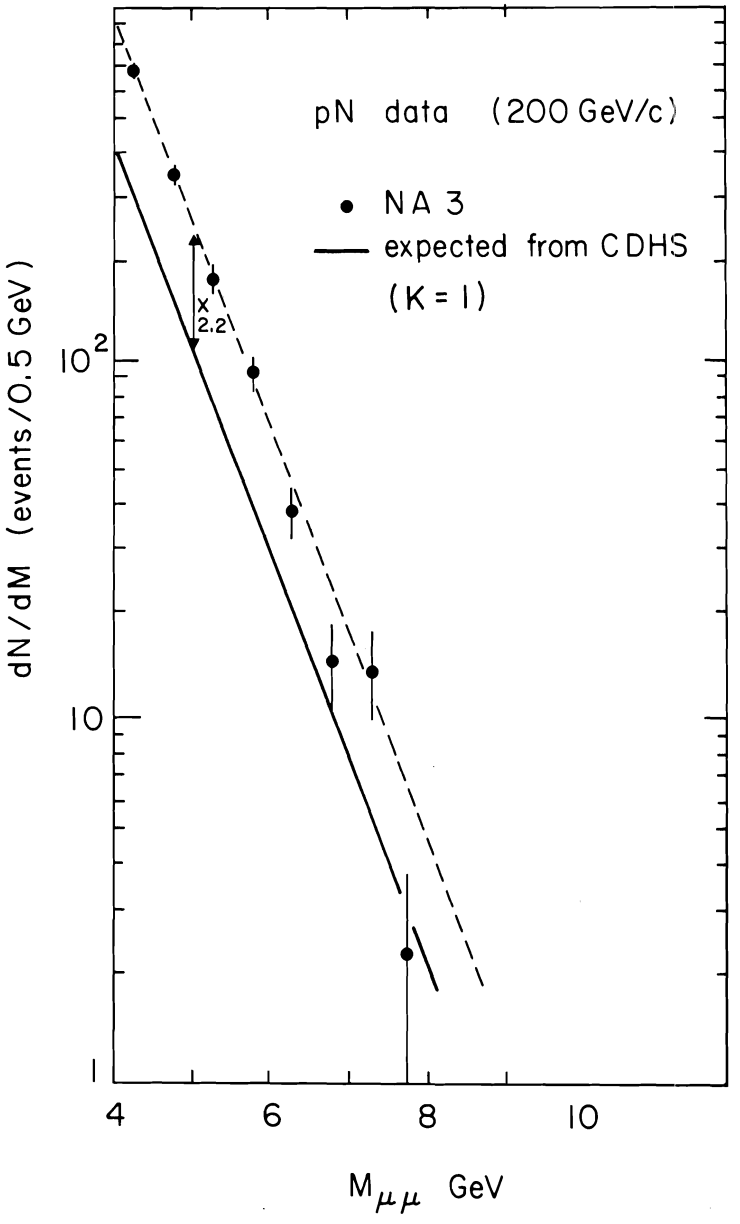

Fig. 12 Mass spectrum for pN events at 200 GeV/c; compared to prediction from CDHS nucleon structure function.

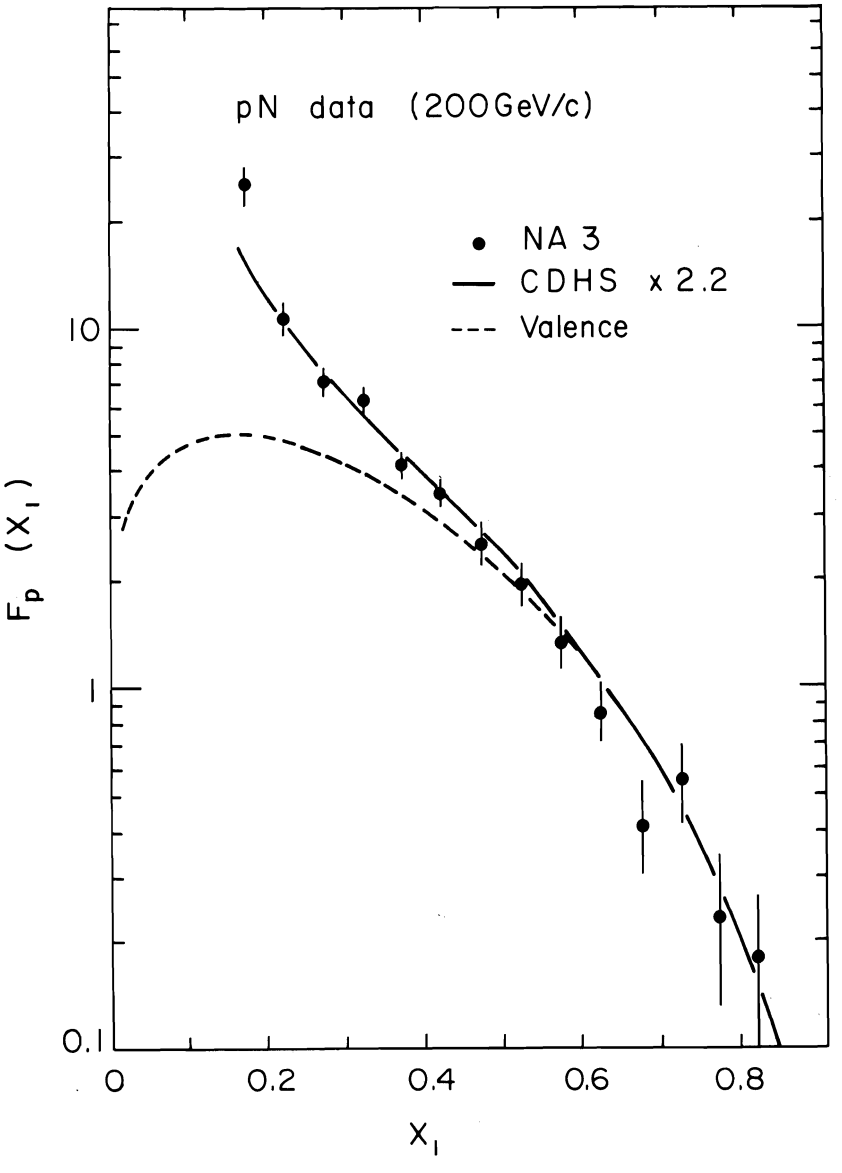

Fig. 13 NA3 proton structure function vs. CDHS at $Q^2 = 20(GeV/c)^2$.

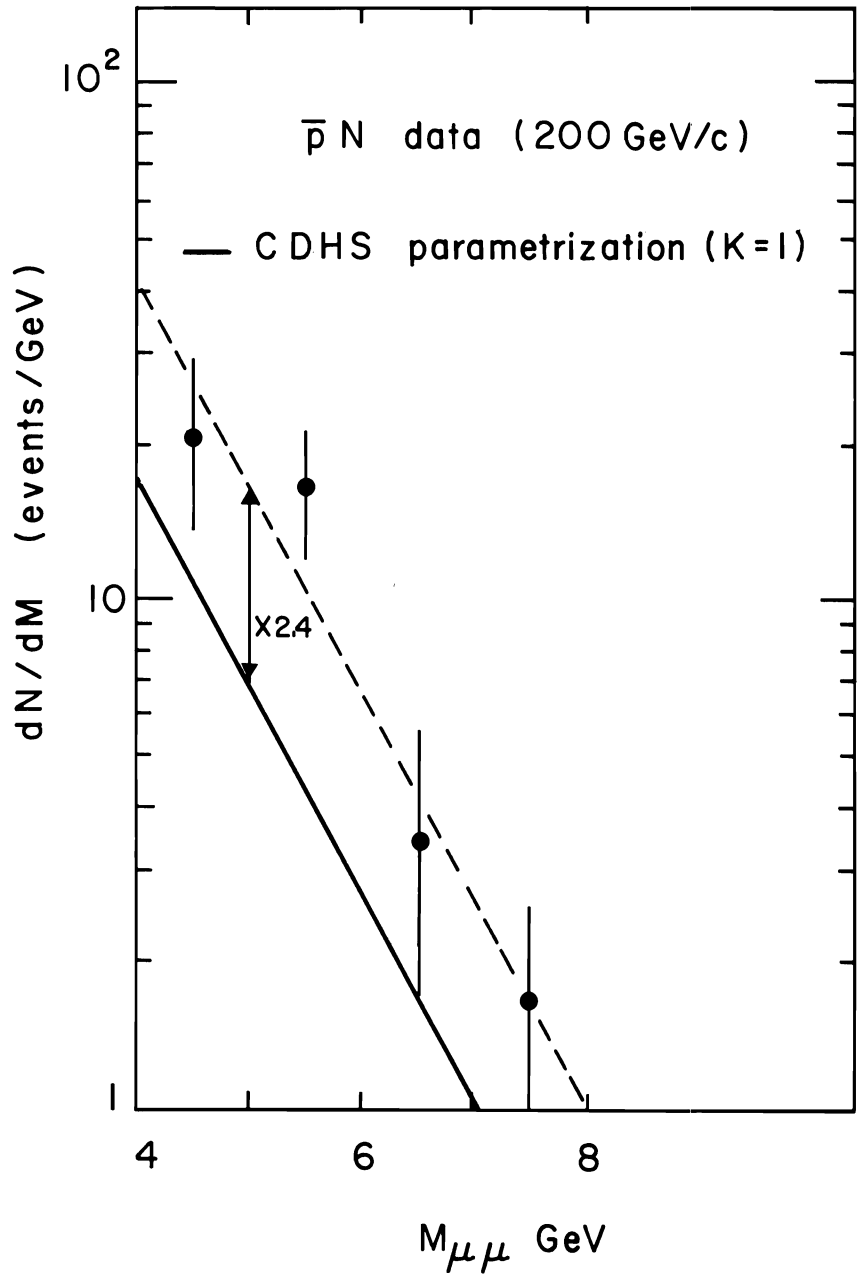

Fig. 14 $\bar{p}$ induced di-muon mass spectra vs. expectation from CDHS data.

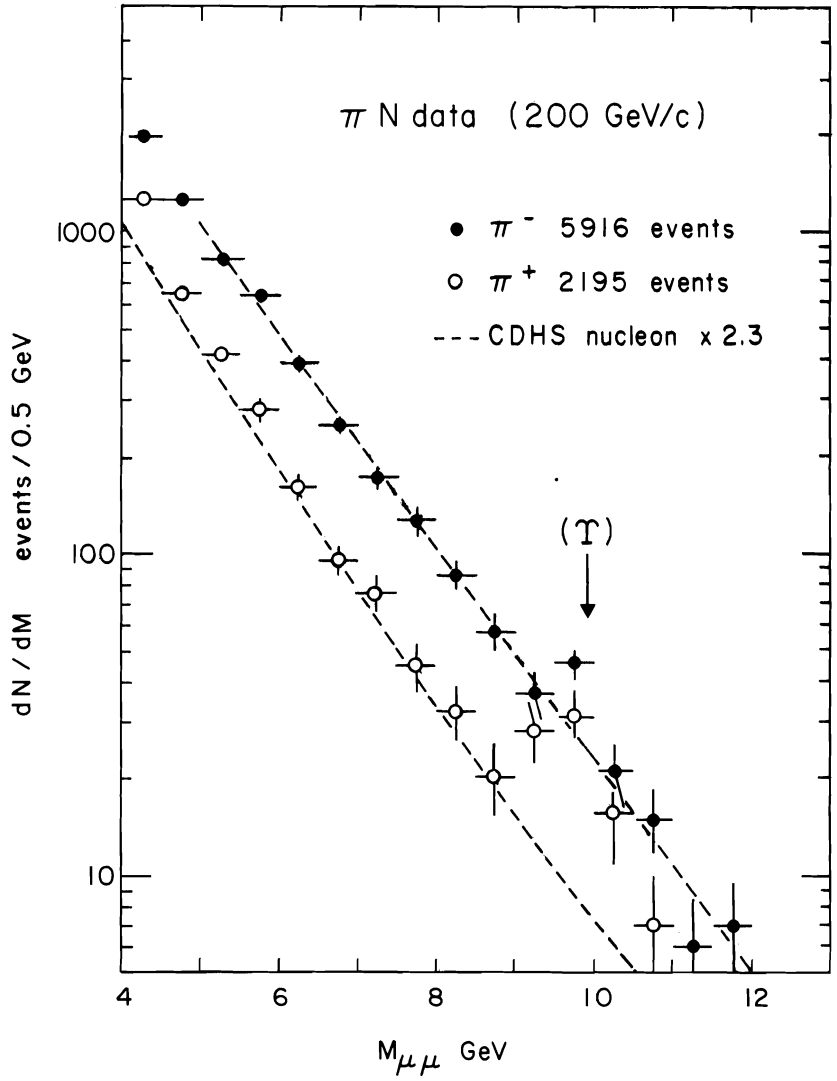

Fig. 15 $\pi^{\pm}$ induced di-muon mass spectrum compared to expectation using CDHS nucleon structure.

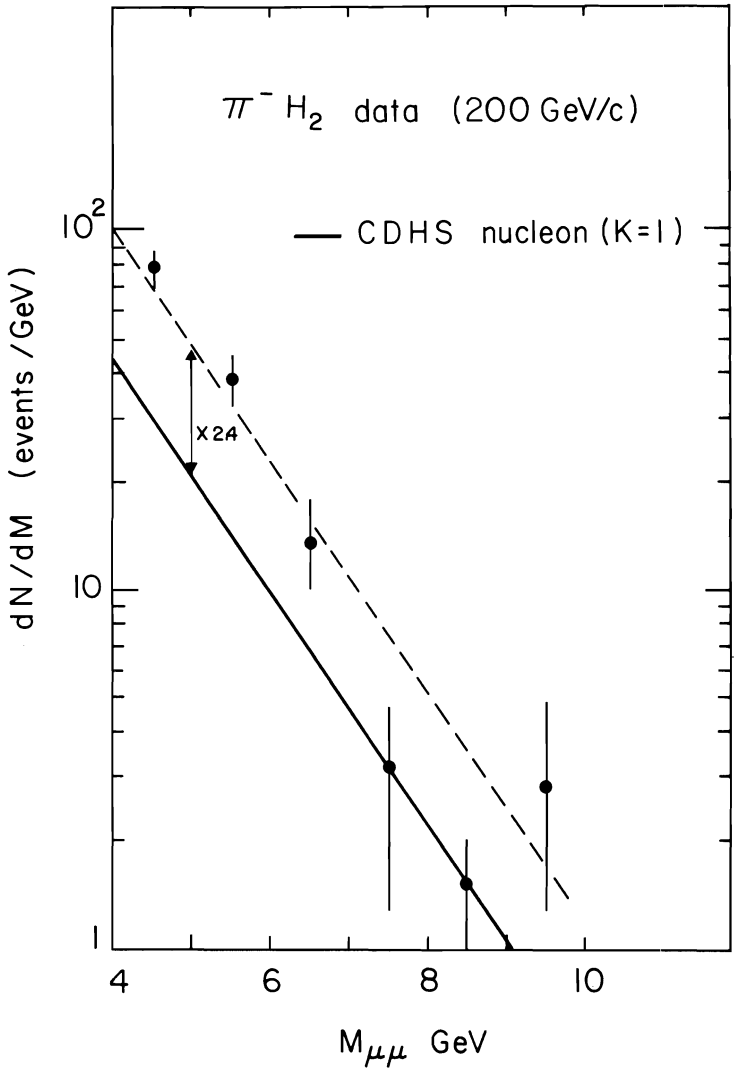

Fig. 16 Di-muon mass spectrum for $\pi^- H_2$ data.

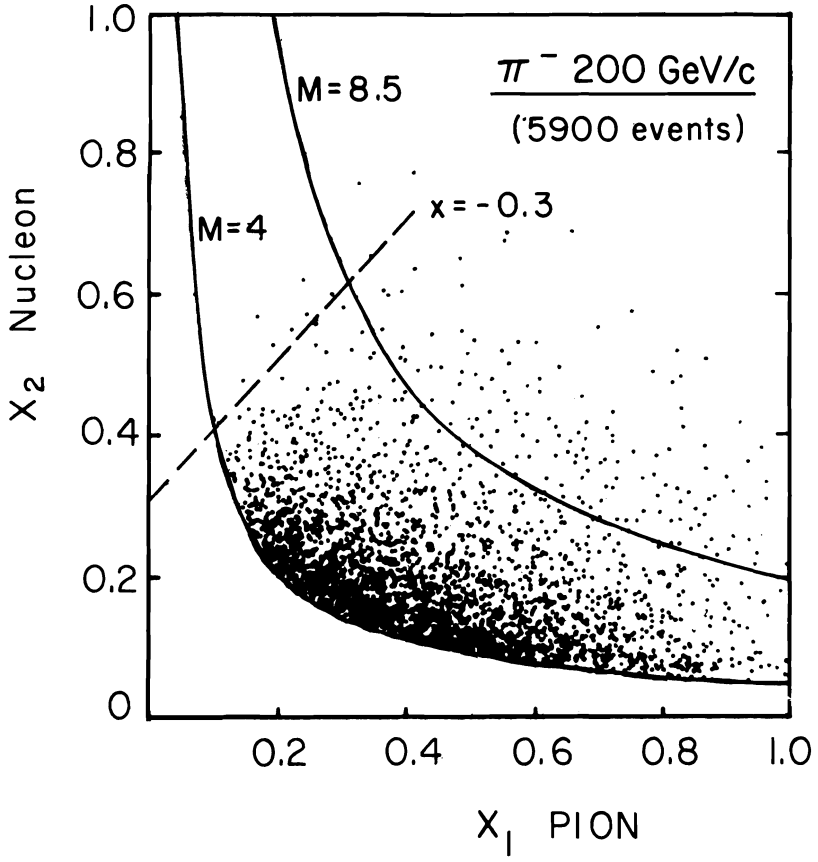

Fig. 17. x_1-x_2 scatter plot for π^- events at 200 GeV/c.

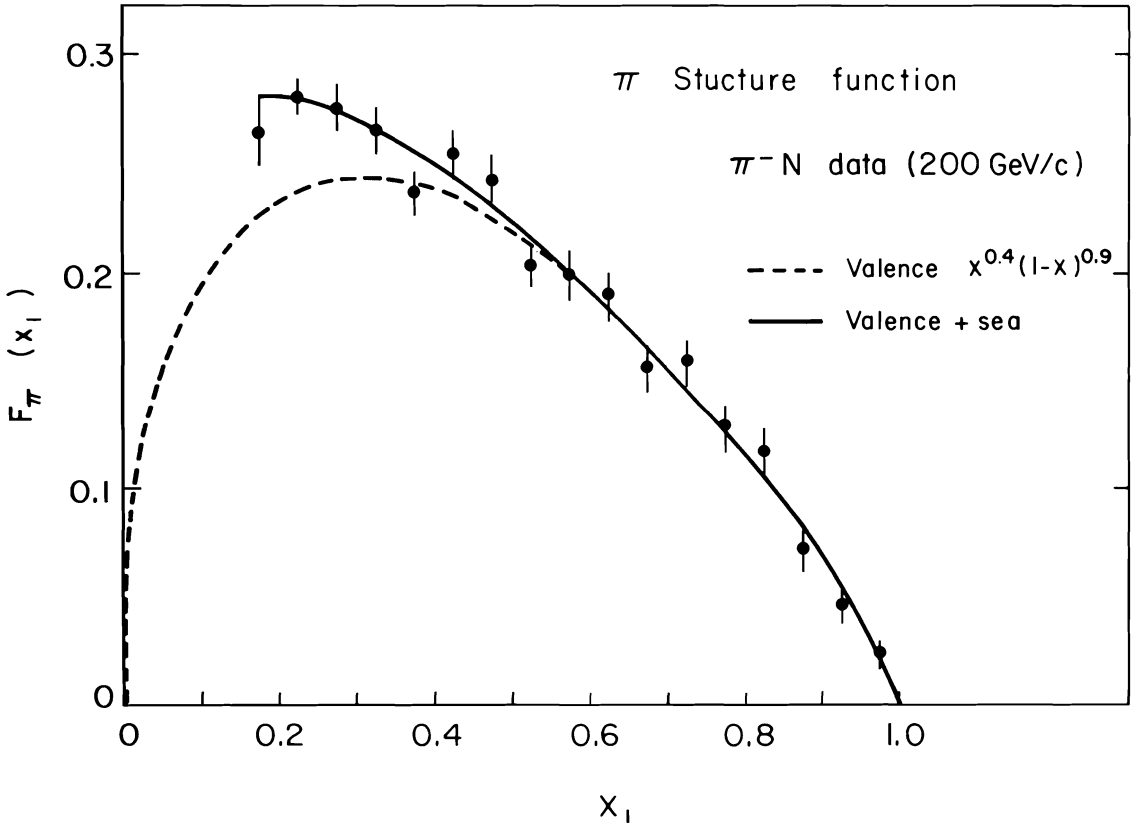

Fig. 18. The π structure function.